3-D-Printing and High-Precision Milling of W-Band Filter Components With Admittance Inverter Sequences

Chad Bartlett, *Student Member, IEEE*, Jens Bornemann, *Life Fellow, IEEE*, and Michael Höft, *Senior Member, IEEE*

***Abstract*— This work presents the design of an additively manufactured W-band bandpass filter and a subtractively manufactured W-band diplexer to demonstrate the use of admittance inverter sequences for the ease of manufacture at millimeter-wave frequencies. Contrary to typical impedance inverters (E-plane and H-plane irises), the use of admittance inverters (E-plane and H-plane stubs) allows for larger dimensions to be specified and ultimately does not impede the general waveguide path. The proposed bandpass filter is designed with all E-plane stubs, while the diplexer is designed with one branch using both E-plane and H-plane stubs as an arbitrary sequence, and the second branch using all H-plane irises. The additively manufactured bandpass filter is fabricated using the most elementary-level stereolithography (SLA)-based methods, demonstrating that a hobbyist-type SLA printer and metallization method can procure exceptional results for millimeter-wave filter designs. The subtractively manufactured diplexer is fabricated using high-precision computer numerical control (CNC) milling to highlight the use of arbitrary inverter sequences in a more complex and robust design profile, while the dispersive transmission zeros that are caused by over-moding of the inverter stubs are used to demonstrate unique isolation characteristics in the upper W-band region. The design concepts, fabrication profiles, simulations, and measurements which are presented in this work highlight a viable option for overcoming miniaturized dimensions in millimeter and submillimeter-wave applications.**

***Index Terms*— Diplexer, fabrication techniques, filter, millimeter-wave, passive components, stereolithography (SLA), W-band, waveguide inverters, WR-10.**

Manuscript received May 10, 2021; revised August 27, 2021; accepted September 22, 2021. Date of publication September 29, 2021; date of current version December 16, 2021. This work was supported by the European Union's Horizon 2020 research and innovation program under the Marie Skłodowska-Curie Grant 811232-H2020-MSCA-ITN-2018. Recommended for publication by Associate Editor D. P. Parekh upon evaluation of reviewers' comments. *(Corresponding author: Jens Bornemann.)*

Chad Bartlett and Michael Höft are with the Institute of Electrical Engineering and Information Engineering, Kiel University, 24118 Kiel, Germany (e-mail: chb@tf.uni-kiel.de; mh@tf.uni-kiel.de).

Jens Bornemann is with the Department of Electrical and Computer Engineering, University of Victoria, Victoria, BC V8W 2Y2, Canada (e-mail: j.bornemann@ieee.org).

Color versions of one or more figures in this article are available at https://doi.org/10.1109/TCPMT.2021.3116220.

Digital Object Identifier 10.1109/TCPMT.2021.3116220

I. Introduction

FUTURE demands for high-data-rate communication systems and constellation micro-satellite networks have triggered an increasing amount of research toward overcoming the challenges of space- and suborbital-based systems. As the electromagnetic spectrum becomes increasingly overcrowded within the lower-frequency bands, use of the millimeter-wave frequency range offers many advantages that can be applied to the next generations of communication, radar, and satellite equipment. These advantages can be viewed not only as reductions in size and weight but also as methods to reduce interference and harness regions with selective atmospheric attenuation [1], [2]. However, the development of components within the millimeter-wave region poses their own inherent challenges such as fabrication accuracy, surface roughness, and suitable design procedures for additive manufacturing. With regard to W-band cavity-based waveguide filter designs, alternative approaches to computer numerical control (CNC) milling have been proposed throughout the literature and have been able to demonstrate a varying degree of measured results. Some of the most recent developments with regard to reported W-band results using additive manufacturing techniques include stereolithography (SLA) [3]–[5], selective laser melting (SLM) [6], selective laser sintering (SLS) [7], and micro-laser sintering (MLS) [8], [9]. In general, each of these techniques approaches overcoming high-frequency fabrication challenges from a technological standpoint rather than from a circuit synthesis approach.

In [10], direct-coupled rectangular waveguide filters with arbitrary inverter sequences were proposed and many new configurations were demonstrated in the Ku-band by simulation. Although half-wave and quarter-wave techniques are well-known, the use of alternating impedance and admittance inverters or all-admittance inverters is still vastly unexplored in the current literature on cavity-based waveguide components. To the authors' knowledge, only simulations proposed in [10] have been applied to demonstrate all-admittance inverter sequences in rectangular waveguide bandpass filter designs. Given that the general structure of admittance inverters is larger than their impedance inverter counterparts, their use in millimeter wave and submillimeter wave designs should be investigated for overcoming fabrication challenges with regard to aspect ratio, etching inconsistencies, and general dimensions that are difficult to obtain. In fact, both additive and subtractive fabrication methods can greatly benefit from the alternative design profiles offered from this method; for example, thin-walled irises and narrow iris gaps which are subject to warping, under-etching, or infeasible milling dimensions can be avoided all together.

To further this line of research, we investigate this method as a means of overcoming difficulties with miniature filter fabrication. The designs which follow are the first examples of waveguide-based filters and diplexers that use inverter sequences to ease the stringent dimensions required in millimeter-wave designs. In this manner, the key underlying theme of this investigation is the use of inductive and capacitive stubs, where inherently the size of the component's coupling inverters is sacrificed as a means of constructing a filter path without impeding (or interceding) the fundamental waveguide dimensions (2.54 mm $\times$ 1.27 mm for a standard WR-10 waveguide). Two inherently different methods of production are used for prototype fabrication, namely, the filter is demonstrated in SLA 3-D-printing as an additively manufactured option and the diplexer is demonstrated using high-precision CNC milling as a subtractively manufactured option. The former method that is used in this study demonstrates a very low-cost option in which a hobbyist-type SLA printer and an elementary copper-based metallization method is used for the fabrication of an all-admittance inverter (E-plane stub) filter. This SLA version of the filter is designed for a passband between 95 and 105 GHz and ultimately demonstrates that a very coarse method of fabrication can easily reach the millimeter-wave frequency range without the need of a commercial-grade SLA printer, (Ni) nickel or (Ag) silver-based plating methods, or the design of complicated slot-structures to allow for internal metallization. The latter method demonstrates the use of high-precision CNC milling to facilitate a more complex and robust mixed-inverter diplexer structure, where the first branch of the diplexer takes the form of an all-admittance inverter filter (E-plane and H-plane stubs), and the second branch of the diplexer takes the form of an all-impedance inverter filter (H-plane irises). The admittance inverter branch is selected as the diplexer's lower passband to use the transmission zeros that are caused by over-moding in the upper region of the W-band. Both the diplexer's passbands are selected for 5 GHz operation, which are designated for the ranges of 95–100 GHz and 103–108 GHz. Each of the components in this work exhibits passband characteristics in the upper portion of the W-band, and both of the experimental prototypes are fabricated with an E-plane cut as split-block designs. A discussion on both of the design's capabilities is presented, and a comparison of the simulated and measured results is discussed to highlight the fabrication and operational characteristics.

II. Design Methodology

As part of any general synthesis procedure, the inverter type and sequence must be selected to facilitate the interconnection between resonator cavities. Fig. 1 depicts four of the basic waveguide inverter forms; Fig. 1(a) and (b) represents H-plane and E-plane admittance inverter stubs, respectively, while Fig. 1(c) and (d) represents H-plane and E-plane impedance inverter irises, respectively. From these representations, it is clear that the admittance inverter stubs shown in Fig. 1(a) and (b) will intrinsically occupy a volume that is outside of the general waveguide dimensions. This in turn has several disadvantages; one being that the overall design becomes less compact, and the second being that over-moding can generate many spurious modes in the rejection-band regions when directly compared with impedance inverter designs [10]. However, in the case of very high-frequency designs, it may be advantageous for designers to use the larger and less restrictive dimensions for overcoming critical or difficult fabrication schemes, especially in the case of additive manufacturing or silicon micro-machining. The following demonstrates two examples which use admittance inverters for W-band operation and use two distinctly different technologies for their inception. For both the designs, the full-wave edge-condition-based coupled-integral equations technique (CIET) based on [11]–[14] and further demonstrated in [10] is used to quickly synthesize and pre-emptively optimize the dimensions of the proposed filter and each of the filtering branches of the diplexer before final optimization in CST Microwave Studio. As part of the final optimization, fabrication considerations are made for E-plane manufacture and the corner radii are taken into account for accurate component profiles. As follows, Section II-A outlines the all-admittance inverter filter for fabrication with a low-cost SLA-printing method, Section II-B outlines the mixed-inverter diplexer for fabrication using high-precision CNC milling, Section III presents a discussion on the fabrication routine and the measured results, Section IV compares the measured results with the state-of-the-art, and Section V serves as a conclusion.

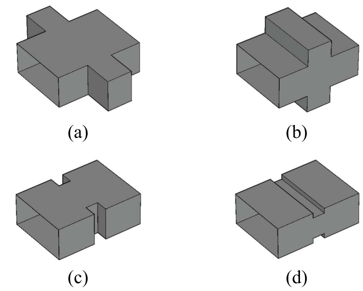

Fig. 1. Basic forms of waveguide inverters. (a) Inductive stub. (b) Capacitive stub. (c) Inductive iris. (d) Capacitive iris.

A. 3-D-Printed Admittance Inverter Filter

For the design of the filter structure, an all-admittance inverter scheme was selected as the method to demonstrate a simple and low-cost method of 3-D-printing at millimeter-wave frequencies. The design procedure starts by obtaining the general Chebyshev coefficients from [15] and determining

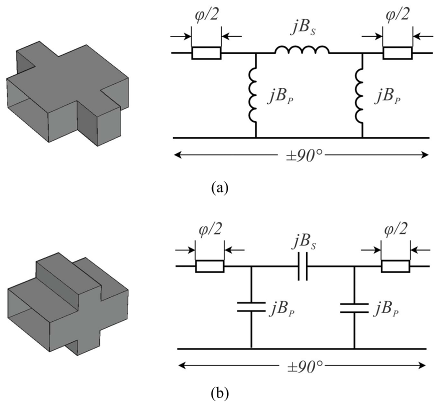

Fig. 2. Waveguide admittance inverters and their corresponding circuit topologies. (a) Inductive stub. (b) Capacitive stub.

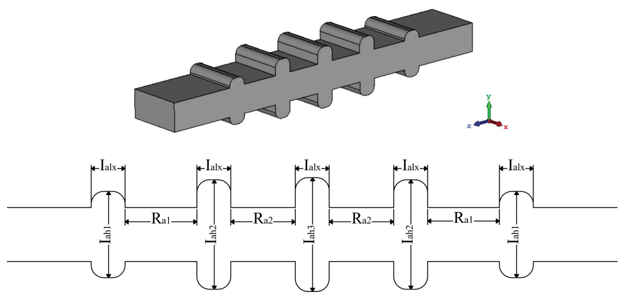

Fig. 3. Perspective view of the admittance-inverter filter's vacuum shell and its corresponding dimensions; $R_{a1} = 1.695$ mm, $R_{a2} = 1.524$ mm, $I_{alx} = 0.800$ mm, $I_{ah1} = 2.032$ mm, $I_{ah2} = 2.578$ mm, and $I_{ah3} = 2.680$ mm.

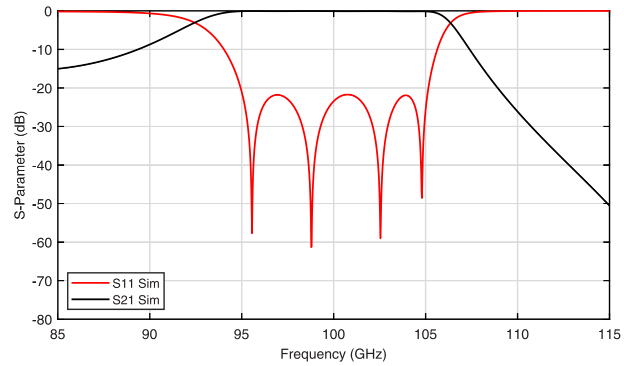

Fig. 4. S-parameters of the simulated admittance-inverter filter (conductivity of copper taken as 5.8×10^7 S/m).

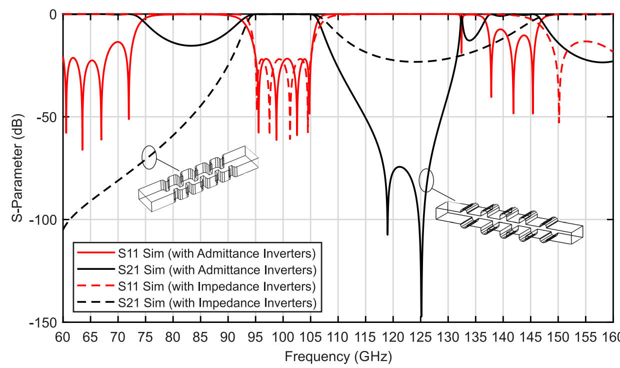

Fig. 5. Wideband spurious performance of the simulated admittance-inverter filter with comparison to an impedance-inverter filter with similar specifications (conductivity of copper taken as 5.8×10^7 S/m).

the normalized inverter values with (1) for the admittance inverter schemes shown in Fig. 2. Equation (2) is applied to adjust the individual resonator lengths between the selected inverters [10].

$$jB_p = \frac{(1-S_{21})^2 - S_{11}^2}{(1+S_{11})^2 - S_{21}^2} \tag{1a}$$

$$jB_s = \frac{2S_{21}}{(1+S_{11})^2 - S_{21}^2} \tag{1b}$$

$$\phi = -\tan^{-1}(2B_s + B_p) - \tan^{-1} B_p \tag{1c}$$

$$J = \left|\tan\left(\frac{\phi}{2} + \tan^{-1} B_p\right)\right| \tag{1d}$$

$$l_i = \frac{\lambda_{g0}}{2\pi}\left[\pi + \frac{1}{2}(\phi_{2,i} + \phi_{1,i+1})\right] \tag{2}$$

For the case at hand, the filter is designed using capacitive stubs [as shown in Fig. 2(b)] to achieve a passband over the 95–105-GHz region. Synthesis based on the CIET is used for the initial design parameters, where the inverter aperture is varied in a search algorithm and the stub thickness is held constant [10], [14]. In this manner, the initial design can be quickly synthesized before a final optimization in CST Microwave Studio. Fig. 3 depicts a perspective view of the admittance inverter filter's vacuum shell and its corresponding dimensions. Fig. 4 exhibits the final simulated S-parameters of the structure depicted in Fig. 3 over the range of 85–115 GHz.

Common to stub inverter designs, the lower rejection-band region has lower selectivity than the upper rejection-band region. This lower selectivity can be overcome using more complex inverter sequences such as demonstrated in [10] and [16]–[18], but for experimental purposes with hobbyist-type SLA-printing, we resolve to first demonstrate the elementary (all-admittance inverter) configuration. The wideband spurious performance of the filter is detailed in Fig. 5 over the range of 60–160 GHz, where in addition, the simulated results are compared with the response of a typical fourth-order impedance inverter (all-inductive iris) filter with similar specifications. The wider range is beyond the definition of the W-band, which is 75–110 GHz. One should be aware that the TE_{20} mode cutoff frequency is at approximately 118 GHz, and therefore, note that slight geometrical asymmetries may excite further modes.

With regard to the proposed admittance-inverter filter design outlined in Fig. 3, a 0.3 mm radius is selected for the inner corners of the inverter stubs; however, it can be noted that the radii of the stubs are an optional feature in this design since the structure is to be additively manufactured. Nevertheless, we choose to incorporate the corner radii, as other designers can use our specified dimensions for either additive or subtractive manufacturing of their own.

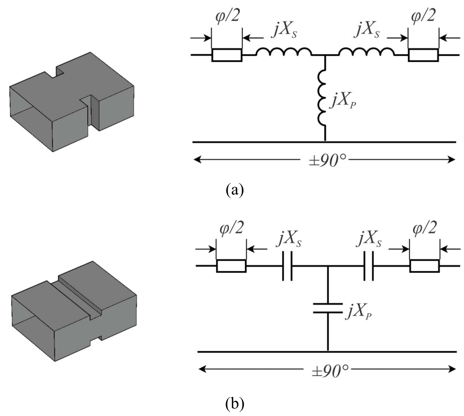

Fig. 6. Waveguide impedance inverters and their corresponding circuit topologies. (a) Inductive iris. (b) Capacitive iris.

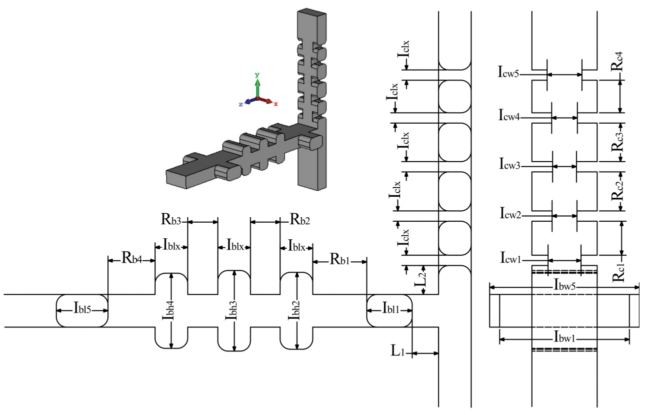

Fig. 7. Perspective view of the mixed-inverter diplexer's vacuum shell and its corresponding dimensions. Admittance inverter branch values: $R_{b1} = 2.102$ mm, $R_{b2} = 1.154$ mm, $R_{b3} = 1.172$ mm, $R_{b4} = 1.832$ mm, $I_{bl1} = 1.768$ mm, $I_{bw1} = 5.050$ mm, $I_{bh2} = 2.990$ mm, $I_{bh3} = 3.134$ mm, $I_{bh4} = 2.920$ mm, $I_{blx} = 1.270$ mm, $I_{bl5} = 2.010$ mm, $I_{bw5} = 5.830$ mm, $L_1 = 1.026$ mm, and impedance inverter branch values: $R_{c1} = 1.321$ mm, $R_{c2} = 1.511$ mm, $R_{c3} = 1.496$ mm, $R_{c4} = 1.266$ mm, $I_{cw1} = 1.282$ mm, $I_{cw2} = 0.968$ mm, $I_{cw3} = 0.930$ mm, $I_{cw4} = 1.000$ mm, $I_{cw5} = 1.356$ mm, $I_{clx} = 0.400$ mm, and $L_2 = 1.125$ mm.

B. High-Precision CNC Milled Mixed-Inverter Diplexer

For the design of the diplexer structure, the two filtering branches were designed separately, but in accordance with either an all-admittance inverter or all-impedance inverter selection. Although these constraints were chosen arbitrarily, it allows for a more academic and investigative exercise when comparing and contrasting the diplexer's capabilities. The design procedure is similar to the one described in Section II-A, but now includes the use of (3) for the impedance inverter schemes that are shown in Fig. 6. The first branch has been selected for the lower passband of the diplexer as an all-admittance inverter design that uses both E-plane and H-plane stubs and follows from (1) and (2). The second branch has been selected for the upper passband of the diplexer as an all-impedance inverter design that uses all H-plane irises and follows from (2) and (3). The lower and upper passbands have been designated for approximately 5 GHz bandwidth each; these passbands are defined from 95–100 GHz and 103–108 GHz, respectively. Synthesis based on the CIET is used for the initial design of each branch before final optimization as a mixed-inverter diplexer unit. Fig. 7 depicts a perspective view of the diplexer's vacuum shell and its corresponding dimensions.

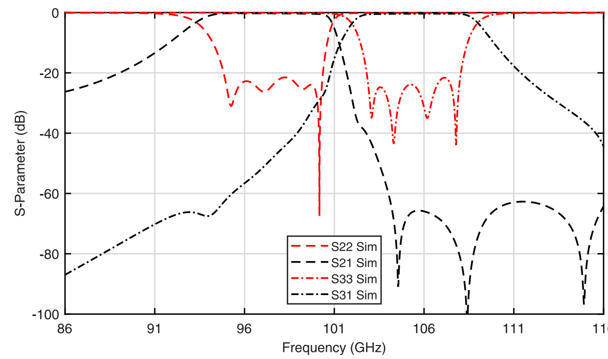

Fig. 8. *S*-parameters of the simulated mixed-inverter diplexer (conductivity of brass taken as 1.59×10^7 S/m).

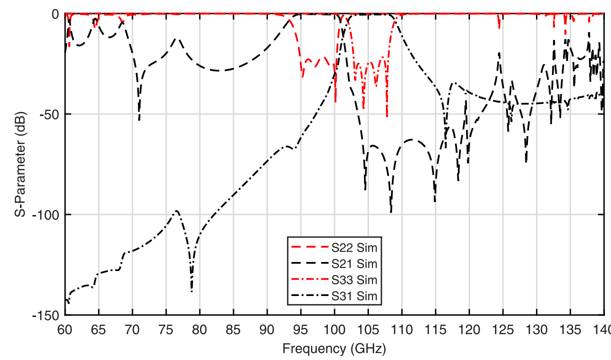

Fig. 9. Wideband spurious performance of the simulated mixed-inverter diplexer (conductivity of brass taken as 1.59×10^7 S/m).

$$jX_s = \frac{(1 - S_{21})^2 - S_{11}^2}{(1 - S_{11})^2 - S_{21}^2} \tag{3a}$$

$$jX_p = \frac{2S_{21}}{(1 - S_{11})^2 - S_{21}^2} \tag{3b}$$

$$\phi = -\tan^{-1}\left(2X_p + X_s\right) - \tan^{-1} X_s \tag{3c}$$

$$K = \left|\tan\left(\frac{\phi}{2} + \tan^{-1} X_s\right)\right| \tag{3d}$$

Fig. 8 exhibits the simulated *S*-parameters over the range of 86–116 GHz. The upper passband takes the form of a standard Chebyshev filter, while the lower passband exhibits dispersive transmission zeros above its passband, which are typical of over-moded inverter stubs [10]. However, this can be advantageous in a diplexing format as shown in this example, since transmission zeros can be allocated without the need of cross-coupling or complex multi-mode designs and simultaneously avoid reduced waveguide height/width requirements that are typically used in advanced diplexing formats, for example, [17]–[24]. Fig. 9 demonstrates the wideband spurious performance of the diplexer over the range of 60–140 GHz, again beyond the definition of the W-band.

III. Fabrication and Measurement

For the fabrication of the filter, an *Elegoo Mars 2 MSLA* 3-D-printer was selected for its nature as a low-cost hobbyist-type tool. The prototype is printed as two separate blocks along the E-plane with a 0.02 mm print-layer height of nonconductive photo-polymer resin. As mentioned in Section II-A,

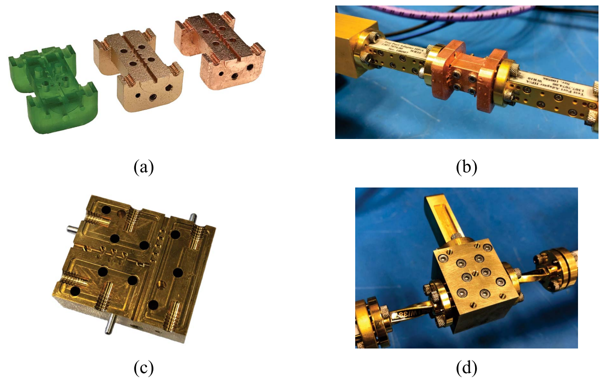

Fig. 10. Fabrication and assembly. (a) Progression of the fabricated admittance-inverter filter; one half of the split block is shown at different stages with respect to the steps outlined in Section III: *3-D-printing of the structure* (left), *post-printing stage 2*; copper spray-coated (center), and after the *galvanization process*; with sufficient metallization (right). (b) Assembled admittance-inverter filter connected to the test bed. (c) One half of the mixed-inverter diplexer after milling (shown along the E-plane). (d) Assembled mixed-inverter diplexer connected to the test bed.

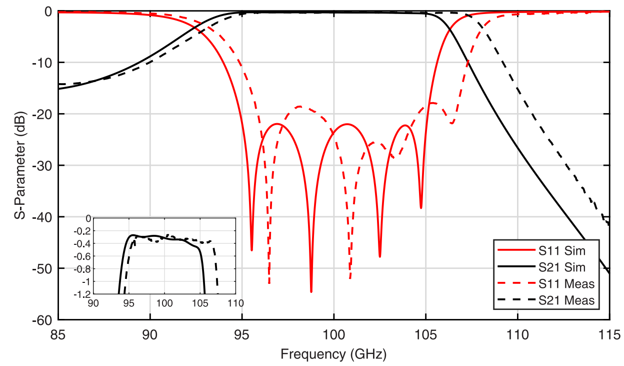

Fig. 11. Simulated versus measured *S*-parameters of the 3-D-printed admittance-inverter filter. The inset shows a close-up view of the insertion loss (equivalent conductivity of copper taken as 4.2×10^6 S/m).

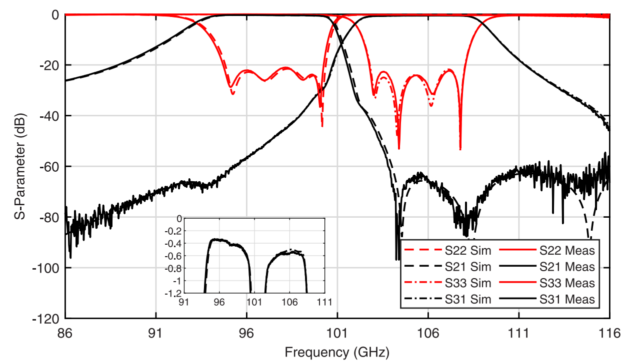

Fig. 12. Simulated versus measured *S*-parameters of the high-precision milled mixed-inverter diplexer. The inset shows a close-up view of the insertion loss in the lower and upper passbands (equivalent conductivity of brass taken as 7.7×10^6 S/m).

a radius of 0.3 mm has been added to the inverter stubs. At this stage in other filter works of this frequency range, an electroless plating method is used to uniformly coat the surfaces of the structure with a nickel-based seed layer for electroplating [3]–[5]. However, by printing the structure in an E-plane format, a low-cost copper-based aerosol spray [25] can be applied to each half of the filter blocks as a precursor, forgoing the need for chemical seed baths, paint-gun spraying equipment, the design of specialized metallization slots for the component's interior structures, or professional printing and metallization services.

In general, copper electroplating is a rather coarse but simple method for plating plastic-based 3-D-printed parts, especially when considering the micro-fine detail required for components at very high frequencies. Additionally, factors such as the enlargement and shrinkage of the component after photo-polymer resin curing must be accounted for in the fabrication process; these factors become highly critical in millimeter-wave design and must be suitably addressed. For the design at hand, it was found that nonuniform scaling factors were required for each of the coordinate directions of the internal filter dimensions. Using the x–y–z coordinates that have been defined in Fig. 3, the scaling factors which have lead to the reported results are 1.07 times along the x-axis, 1.12 times along the y-axis, and 1.00 times along the z-axis. These scaling factors were determined through trial and error and are applied to the SLA-printed structure to balance the enlargement and shrinkage associated with curing of photo-polymer resin, the copper spray coating, and the final electroplating layer. The following outlines the general fabrication process, while Fig. 10(a) depicts the progression of the filter at several different stages of fabrication.

1) 3-D Printing of the structure: For the case at hand, an *Elegoo Mars 2* has been selected for low-cost SLA printing with a print-layer height of 0.02 mm. After the structure is printed, it is cleaned with isopropyl alcohol to remove excess resin and then cured for 8 min in UV light.

2) Post-printing stage 1: The threads of the flange holes are threaded by hand and the structure is cleaned with galvano degreaser and distilled water and then left to air dry.

3) Post-printing stage 2: Primary and secondary layers of copper aerosol spray are applied for approximately 1–2 s for each pass until all the resin is coated. The sprayed coating is left to dry for 12 h.

4) Galvanization process: Electroplating is conducted in acidic copper electrolyte for 2 h at 400 mA with a distance of 85 mm from the cathode. After removal, the structure is cleaned with distilled water, dried, and the flange threads are re-tapped to clean out excess copper and debris.

5) Quality control: Mechanical (caliper) and electrical (VNA) measurements are made to test the structure. Poor metallization or measurements require the vacuum structure and/or housing to be scaled accordingly. The process is reiterated from Step 1 until the desired specifications are met.

Upon reaching the *Quality Control* stage of the fabrication process outlined above, the two filter halves are fastened together by mounting-screws through each half of the component body [as shown in Fig. 10(b)]. The pliability and the fine surface finish of the 3-D-printed part allow for the two halves to be compressed adequately and allow for any localized air gaps to be mitigated. Measurement of the filter allows for errors to be identified and corrected in an iterative fabrication process. For example; a deviation in the

TABLE I
COMPARISON OF W-BAND SLA-FABRICATED BANDPASS FILTERS†

f_c (GHz)	FBW	Insertion loss (dB)	Return loss (dB)	Commercial grade 3D-printing	Metallization technique	Construction profile	Reference
87.5	11.5%	0.3 - 0.5	>18	Yes	Ni Electroless & Cu/Au Electroplating	Mono-block	[4]
102.5	3.6%	1.0 - 2.0	<10	Yes	Ni Electroless & Cu Electroplating	Mono-block	[5]
107.2	6.34%	0.95*	>11	Yes	Ni Electroless & Cu Electroplating	Split-block	[3]
101.14	11.10%	0.26 - 0.48	>17	No	Cu aerosol spray & Cu Electroplating	Split-block	This work

TABLE II
COMPARISON OF W-BAND CNC-BASED FABRICATED DIPLEXERS†

f_c (GHz)	FBW	Insertion loss (dB)	Return loss (dB)	Design type	Component parts	Reference
95.5 / 106.5	11.52% / 10.33%	1.5 / 1.7*	NA**	Substrate based fin-line	3	[26]
87.5 / 102.5	5.71% / 4.89/%	1.0 / 1.0*	>10	Substrate based fin-line	3	[27]
90.0 / 110.0	11.11% / 9.09%	1.0 / 1.0*	>12	Substrate based fin-line	3	[27]
97.5 / 105.4	5.62% / 4.99%	0.34 - 0.76 / 0.55 - 0.88	>21	Direct coupled mixed inverter	2 (Split-block)	This work

†Table values are estimated as best as possible for the presented measured data where not directly reported. *Measured data was reported as the achieved typical values or at center frequency (rather than a range), **Data not available.

measured center frequency can require a re-scaling of the filter dimensions, or conversely, poor measured insertion loss can require a thicker metallization layer, where the electroplating duration and current can be adjusted and the structure re-scaled accordingly. Iterations can be made to adjust the process until the desired response is met.

A comparison of the simulated and measured results over the range of 85–115 GHz is presented in Fig. 11 while Fig. 10(b) depicts the filter connected to the test bed. This comparison demonstrates good measured results; the measured return loss is better than 17 dB throughout the passband, and the measured insertion loss is in the range of 0.26–0.48 dB, ultimately, demonstrating that a very coarse method of fabrication and metallization can be applied to achieve good results when compared with other W-band SLA-printed designs that use more professional or commercial-based methods [3]–[5]. The measured surface roughness (S_a) is found to be approximately 3 μm, where S_a describes the mean arithmetic height. With regard to the deviation between the simulated and measured results, this difference can be attributed to several factors such as small misalignments, suboptimal dimensional scaling, and nonuniform metallization thicknesses. However, as discussed previously, more iterations can be applied during the fabrication process to reach the optimal desired performance and further reduce the shift in the measured center frequency.

For the fabrication of the diplexer, brass has been selected as the cutting material due to its machinability and final surface finish. The prototype is split into two separate blocks along the E-plane for high-precision CNC milling. The E-plane has been selected as the optimal cutting plane as it is known to minimize the disturbances of the surface current distribution and reduce the passive intermodulation (PIM) effects in high-power applications [19]. The milling radius for both the diplexer branches has been set to 0.4 mm. Fig. 10(c) and (d) depicts the internally milled structures of the diplexer and the fully assembled unit connected to the test bed. No silver or gold coating has been applied to the structure. The measured surface roughness S_a is found to be approximately 1 μm.

A comparison of the simulated and measured results of the diplexer is presented in Fig. 12 over 86–116 GHz. This comparison demonstrates good measured results in both the passbands. The measured return loss is better than 21 dB throughout both the lower and upper passbands while the measured insertion losses are in the range of 0.34–0.76 dB and 0.55–0.88 dB for the lower and upper passbands, respectively. Although the passbands are slightly different with respect to final bandwidth and center frequency, they are still relatively similar enough to note that for both the simulated and measured results, the admittance inverter branch exhibits a slightly better insertion loss value when compared with the impedance inverter branch. This difference in insertion loss is approximately 0.14 dB when comparing the measured center frequencies of 97.5 and 105.4 GHz and is highlighted in the inset of Fig. 12 over a range of 91–111 GHz.

IV. LITERATURE COMPARISON

For both the filter and the diplexer, a comparison is made to fabricated W-band prototypes of the same technologies in the current literature. Although there are few to be compared at this time, an attempt is made to make a direct comparison between the key differences in fabrication style and measured results for WR-10 profiles. Table I highlights the existing W-band SLA-printed filters, while Table II highlights the existing W-band CNC-based filters. In both the cases, competitive results can be observed; for the SLA filter, a low insertion loss has been achieved using low-cost 3D-printing and metallization techniques, while the high-precision milled diplexer exhibits low insertion losses in a unique split-block profile. Furthermore, the filter and the lower passband branch of the diplexer remain free of any intersection of the base waveguide dimensions.

V. Conclusion

The first instances of a 3-D-printed filter and high-precision CNC milled diplexer that use arbitrary inverter sequences are reported for operation in the W-band. Examination of the models demonstrates the use of admittance inverters and their potential use in future millimeter and submillimeter-wave frequencies. The filter which has been presented has for the first time been fabricated using a low-cost and coarse method to demonstrate the use of a hobbyist 3-D-printing and metallization technique to reach the 100-GHz region, while the diplexer which has been presented has been fabricated using high-precision CNC milling to demonstrate a unique design profile that contrasts the subtle differences between all-admittance and all-impedance inverter models. This work depicts two of the few instances of arbitrary inverter sequences for waveguide design in the literature and exhibits their potential use for overcoming fabrication challenges in micro-scale designs. Future exploration of this topic can aim to include many new designs for overcoming size constraints, difficult fabrication profiles, multipaction, and stringent responses, as well as promote low-cost research options for academic and commercial enterprises.

References

[1] R. Prasad, *5G Outlook Innovations and Applications*. Delft, The Netherlands: River Publishers, 2016.

[2] Y. Balal and Y. Pinhasi, "Atmospheric effects on millimeter and sub-millimeter (THz) satellite communication paths," *J. Infr., Millim., THz Waves*, vol. 40, no. 2, pp. 219–230, Feb. 2019.

[3] M. D'Auria *et al.*, "3-D printed metal-pipe rectangular waveguides," *IEEE Trans. Compon., Packag., Manuf. Technol.*, vol. 5, no. 9, pp. 1339–1349, Sep. 2015.

[4] X. Shang *et al.*, "W-band waveguide filters fabricated by laser micromachining and 3-D printing," *IEEE Trans. Microw. Theory Techn.*, vol. 64, no. 8, pp. 2572–2580, Aug. 2016.

[5] C. Guo *et al.*, "Novel microwave/millimeter-wave passive waveguide devices based on 3-D printing techniques," *J. Infr. Millim. Waves*, vol. 36, no. 1, pp. 81–91, 2017.

[6] B. Zhang and H. Zirath, "3D printed iris bandpass filters for millimetre-wave applications," *Electron. Lett.*, vol. 51, no. 22, pp. 1791–1793, Oct. 2015.

[7] K. Fujiwara, R. Kobayashi, S. Kuwahara, S. Takemura, K. Takizawa, and Y. Watanabe, "3-D printed iris waveguide filter in W-band," in *Proc. 23rd Int. Microw. Radar Conf. (MIKON)*, Oct. 2020, pp. 346–349.

[8] M. Salek *et al.*, "W-band waveguide bandpass filters fabricated by micro laser sintering," *IEEE Trans. Circuits Syst. II, Exp. Briefs*, vol. 66, no. 1, pp. 61–65, Jan. 2019.

[9] M. Salek *et al.*, "90 GHz micro laser sintered filter: Reproducibility and quality assessment," in *Proc. 49th Eur. Microw. Conf. (EuMC)*, Oct. 2019, pp. 296–299.

[10] Q. Wang and J. Bornemann, "Synthesis and design of direct-coupled rectangular waveguide filters with arbitrary inverter sequence," in *Proc. 16th Int. Symp. Antenna Technol. Appl. Electromagn. (ANTEM)*, Jul. 2014, pp. 1–6.

[11] J. Uher, J. Bornemann, and U. Rosenberg, *Waveguide Components for Antenna Feed Systems: Theory and CAD*. Norwood, MA, USA: Artech House, 1993.

[12] S. Amari, J. Bornemann, and R. Vahldieck, "Accurate analysis of scattering from multiple waveguide discontinuities using the coupled-integral equations technique," *J. Electromagn. Waves Appl.*, vol. 10, no. 12, pp. 1623–1644, Jan. 1996.

[13] S. Amari, J. Bornemann, and R. Vahldieck, "Fast and accurate analysis of waveguide filters by the coupled-integral-equations technique," *IEEE Trans. Microw. Theory Techn.*, vol. 45, no. 9, pp. 1611–1618, Sep. 1997.

[14] J. Bornemann, U. Rosenberg, S. Amari, and R. Vahldieck, "Edge-conditioned vector basis functions for the analysis and optimization of rectangular waveguide dual-mode filters," in *IEEE MTT-S Int. Microw. Symp. Dig.*, Jun. 1999, pp. 1695–1698.

[15] G. L. Matthaei, L. Young, and E. M. T. Jones, *Microwave Filters, Impedance-Matching Networks, and Coupling Structures*. Norwood, MA, USA: Artech House, 1980.

[16] S. Zhang and L. Zhu, "Synthesis method for even-order symmetrical Chebyshev bandpass filters with alternative J/K inverters and $\lambda/4$ resonators," *IEEE Trans. Microw. Theory Techn.*, vol. 61, no. 2, pp. 808–816, Feb. 2013.

[17] W. Menzel, F. Alessandri, A. Plattner, and J. Bornemann, "Planar integrated waveguide diplexer for low-loss millimeter-wave applications," in *Proc. 27th Eur. Microw. Conf.*, Jerusalem, Israel, Sep. 1997, pp. 676–680.

[18] S. Amari, J. Bornemann, W. Menzel, and F. Alessandri, "Diplexer design using pre-synthesized waveguide filters with strongly dispersive inverters," in *IEEE MTT-S Int. Microw. Symp. Dig.*, May 2001, pp. 1627–1630.

[19] S. Hyeun Yun, M. Seok Uhm, and I. Bok Yom, "Design of the multipaction free high power Ka-band diplexer with an E-plane T-junction," in *Proc. Asia–Pacific Conf. Commun.*, Oct. 2005, pp. 582–585.

[20] F. Teberio *et al.*, "Compact broadband waveguide diplexer for satellite applications," in *IEEE MTT-S Int. Microw. Symp. Dig.*, May 2016, pp. 1–4.

[21] F. Teberio, I. Arregui, P. Soto, M. A. G. Laso, V. E. Boria, and M. Guglielmi, "High-performance compact diplexers for Ku/K-band satellite applications," *IEEE Trans. Microw. Theory Techn.*, vol. 65, no. 10, pp. 3866–3876, Oct. 2017.

[22] U. Rosenberg, A. Bradt, M. Perelshtein, and P. Bourbonnais, "Extreme broadband waveguide diplexer design for high performance antenna feed systems," in *Proc. Eur. Microw. Conf. (EuMC)*, Paris, France, Sep. 2010, pp. 1249–1252.

[23] J. R. Aitken and J. Hong, "Design of millimetre wave diplexers with relaxed fabrication tolerances," *IET Microw., Antennas Propag.*, vol. 9, no. 8, pp. 802–807, Jun. 2015.

[24] H. Setti, A. Tribak, A. El Hamichi, L. Yechou, and A. Mediavilla, "Design and manufacture of a diplexer for K/Ka band satellite applications," *Int. J. Sci. Eng. Res.*, vol. 9, no. 10, pp. 914–918, 2018.

[25] *Tifoo Shop*. Accessed: Apr. 13, 2021. [Online]. Available: https://www.tifoo.de/

[26] C. Nguyen and K. Chang, "Design and performance of a W-band broadband finline diplexer with over 20 GHz bandwidth," in *IEEE MTT-S Int. Microw. Symp. Dig.*, Jun. 1985, pp. 349–352.

[27] Y.-C. Shih, L. Q. Bui, and T. Itoh, "Millimeter-wave diplexers with printed circuit elements," *IEEE Trans. Microw. Theory Techn.*, vol. MTT-33, no. 12, pp. 1465–1469, Dec. 1985.

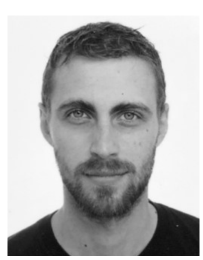

Chad Bartlett (Student Member, IEEE) was born in Nelson, BC, Canada, in 1987. He received the B.Eng. and M.A.Sc. degrees in electrical engineering from the University of Victoria, Victoria, BC, in 2017 and 2019, respectively. He is currently pursuing the Dr.-Ing. degree at the Chair of Microwave Engineering, Institute of Electrical Engineering and Information Engineering, University of Kiel, Kiel, Germany.

His primary research interests include microwave and millimeter-wave passive components, filters, and antenna networks for the next generation of satellite and communication systems, as well as developing methods for overcoming challenges in micro-scale designs.

Mr. Bartlett is a member of the European Union's Horizon 2020 research and innovation program for early-stage researchers.

Jens Bornemann (Life Fellow, IEEE) received the Dipl.-Ing. and Dr.-Ing. degrees in electrical engineering from the University of Bremen, Bremen, Germany, in 1980 and 1984, respectively.

From 1984 to 1985, he worked as an Engineering Consultant. In 1985, he joined the University of Bremen as an Assistant Professor. Since April 1988, he has been with the Department of Electrical and Computer Engineering, University of Victoria, Victoria, BC, Canada, where he became a Professor in 1992. In 1996, he was a Visiting Scientist at Spar Aerospace Limited (now MDA Space), Ste-Anne-de-Bellevue, Quebec, Canada, and a Visiting Professor at the Microwave Department, University of Ulm, Ulm, Germany. From 1997 to 2002, he was a Co-Director of the Center for Advanced Materials and Related Technology (CAMTEC), University of Victoria. In 2003, he was a Visiting Professor at the Laboratory for Electromagnetic Fields and Microwave Electronics, ETH Zurich, Switzerland. He has coauthored *Waveguide Components for Antenna Feed Systems—Theory and Design* (Artech House, 1993) and has authored/coauthored more than 350 technical papers. His research activities include RF/wireless/microwave/millimeter-wave components and systems design, and field-theory-based modeling of integrated circuits, feed networks, and antennas.

Dr. Bornemann is a Registered Professional Engineer in the Province of British Columbia, Canada. He is a fellow of the Canadian Academy of Engineering (CAE) and a fellow of the Engineering Institute of Canada (EIC) and serves on the editorial advisory board of the *International Journal of Numerical Modeling*. From 1992 to 1995, he was a fellow of the British Columbia Advanced Systems Institute. From 1999 to 2002, he served as an Associate Editor of the IEEE TRANSACTIONS ON MICROWAVE THEORY AND TECHNIQUES in the area of Microwave Modeling and CAD. From 2006 to 2008, he was an Associate Editor of the *International Journal of Electronics and Communications*. From 1999 to 2009, he served on the Technical Program Committee of the IEEE MTT-S International Microwave Symposium.

Michael Höft (Senior Member, IEEE) was born in Lübeck, Germany, in 1972. He received the Dipl.-Ing. degree in electrical engineering and the Dr.-Ing. degree from Hamburg University of Technology, Hamburg, Germany, in 1997 and 2002, respectively.

From 2002 to 2013, he joined the Communications Laboratory, European Technology Center, Panasonic Industrial Devices Europe GmbH, Lüneburg. He was a Research Engineer and then the Team Leader, where he had been engaged in research and development of microwave circuitry and components, particularly filters for cellular radio communications. From 2010 to 2013, he was the Group Leader of research and development of sensor and network devices. Since October 2013, he has been a Full Professor with the Faculty of Engineering, University of Kiel, Kiel, Germany, where he is currently the Head of the Microwave Group, Institute of Electrical Engineering and Information Engineering. His research interests include active and passive microwave components, submillimeter-wave quasioptical techniques and circuitry, microwave and field measurement techniques, microwave filters, microwave sensors, and magnetic field sensors.

Dr. Höft is a member of the European Microwave Association (EuMA), the Association of German Engineers (VDI), and the German Institute of Electrical Engineers (VDE).